Many-body localization edge in the random-field Heisenberg chain

David J. Luitz,[*] Nicolas Laflorencie,[†] and Fabien Alet[‡]

Laboratoire de Physique Théorique, IRSAMC, Université de Toulouse, CNRS, 31062 Toulouse, France
(Received 6 November 2014; published 9 February 2015)

We present a large-scale exact diagonalization study of the one-dimensional spin-1/2 Heisenberg model in a random magnetic field. In order to access properties at varying energy densities across the entire spectrum for system sizes up to $L = 22$ spins, we use a spectral transformation which can be applied in a massively parallel fashion. Our results allow for an energy-resolved interpretation of the many-body localization transition including the existence of an extensive many-body mobility edge. The ergodic phase is well characterized by Gaussian orthogonal ensemble statistics, volume-law entanglement, and a full delocalization in the Hilbert space. Conversely, the localized regime displays Poisson statistics, area-law entanglement, and nonergodicity in the Hilbert space where a true localization never occurs. We perform finite-size scaling to extract the critical edge and exponent of the localization length divergence.

Introduction. The interplay of disorder and interactions in quantum systems can lead to several intriguing phenomena, amongst which the so-called many-body localization has attracted a huge interest in recent years. Following precursors works [1–4], perturbative calculations [5,6] have established that the celebrated Anderson localization [7] can survive interactions, and that for large enough disorder, many-body eigenstates can also "localize" (in a sense to be detailed later) and form a new phase of matter commonly referred to as the many-body localized (MBL) phase.

The enormous boost of interest for this topic in recent years can probably be ascribed to the fact that the MBL phase challenges the very foundations of quantum statistical physics, leading to striking theoretical and experimental consequences [8,9]. Several key features of the MBL phase can be highlighted as follows. It is nonergodic, and breaks the eigenstate thermalization hypothesis (ETH) [10–12]: A closed system in the MBL phase does not thermalize solely following its own dynamics. The possible presence of a many-body mobility edge (at a finite energy density in the spectrum) indicates that conductivity should vanish in a finite temperature range in a MBL system [5,6]. Coupling to an external bath will eventually destroy the properties of the MBL phase, but recent arguments show that it can survive and be detected using spectral signatures for weak bath coupling [13]. This leads to the suggestion that the MBL phase can be characterized experimentally, using e.g., controlled echo experiments on reasonably well-isolated systems with dipolar interactions [14–17]. Another appealing aspect (with experimental consequences for self-correcting memories) is that MBL systems can sustain long-range, possibly topological, order in situations where equilibrated systems would not [18–22]. Finally, a striking phenomenological approach [23] pinpoints that the MBL phase shares properties with integrable systems, with an extensive number of local integrals of motion [24–26], and that MBL eigenstates sustain low (area-law) entanglement. This is in contrast with eigenstates at finite energy density

in a generic equilibrated system, which have a large amount (volume law) of entanglement and which are believed to be well described within a random matrix theory approach.

Going beyond perturbative approaches, direct numerical simulations of disordered quantum interacting systems provide a powerful framework to test MBL features in a variety of systems [14,17,21,27–42]. The MBL transition dealing with eigenstates at high(er) energy, ground-state methods are not well adapted. Most numerical studies use full exact diagonalization (ED) to obtain all eigenstates and energies and are limited to rather small Hilbert-space sizes dim $\mathcal{H} \sim 10^4$ [43].

In this Rapid Communication, we present an extensive numerical study of the periodic $S = \frac{1}{2}$ Heisenberg chain in
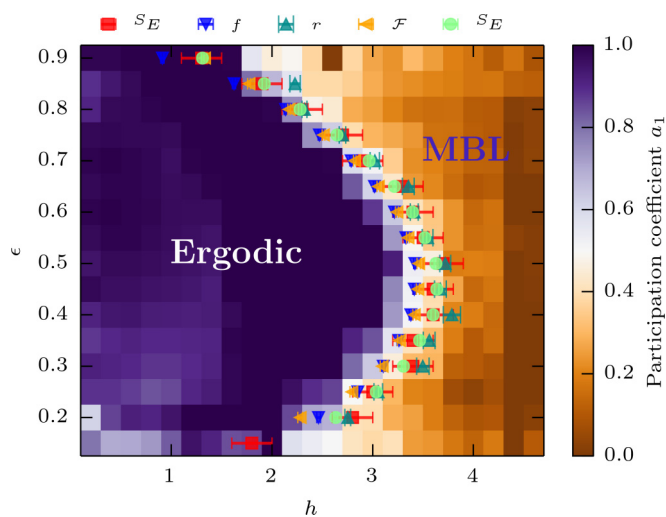

FIG. 1. (Color online) Disorder (h)—Energy density (ϵ) phase diagram of the disordered Heisenberg chain, Eq. (1). The ergodic phase (dark region with a participation entropy volume law coefficient $a_1 \simeq 1$) is separated from the localized regime (bright region with $a_1 \ll 1$). Various symbols (see legend) show the energy-resolved MBL transition points extracted from finite-size scaling performed over system sizes $L \in \{14,15,16,17,18,19,20,22\}$. Red squares correspond to a visual estimate of the boundary between volume and area-law scaling of entanglement entropy S_E.

---

[*]luitz@irsamc.ups-tlse.fr
[†]laflo@irsamc.ups-tlse.fr
[‡]alet@irsamc.ups-tlse.fr

a random magnetic field, governed by the Hamiltonian

$$H = \sum_{i \in [1,L]} \mathbf{S}_i \cdot \mathbf{S}_{i+1} - h_i S_i^z, \tag{1}$$

with h_i drawn from a uniform distribution $[-h,h]$ (total magnetization S^z is conserved). Model (1) has been used [21,28,33,41] as a prototype for the MBL transition in the "infinite-temperature" limit, where the full many-body spectrum (or a large fraction thereof) is considered for systems of maximum size $L \approx 16$. In this work, we instead use a shift-inverse ED approach and are able to reach eigenstates at arbitrary energy density for systems up to $L = 22$ with very large Hilbert spaces (dim $\mathcal{H}_{L=22} = 705\,432$ in the $S^z = 0$ sector). Our simulations unambiguously reveal the existence of an extensive many-body localization edge: The resulting phase diagram (disorder strength h vs energy density ϵ; Fig. 1) is built on a careful finite-size scaling analysis of numerous energy-resolved estimates. In particular, the transition is captured using, e.g., spectral statistical correlations between nearby eigenstates, volume vs. area law of entanglement entropies and bipartite fluctuations, spin relaxation, and localization properties in the Hilbert space, which all roughly agree within error bars. We also perform a scaling analysis close to the MBL transition.

Characterization of ergodic and localized regimes. Before presenting our numerics, we summarize the main differences between ergodic and localized phases, and the observables used to quantify them.

(a) Level statistics and eigenvectors similarity. A popular way to differentiate extended and localized regimes relies on studying spectral statistics using tools from random matrix theory [44]. In the ergodic regime, the statistical distribution of level spacings follows Wigner's surmise of the Gaussian orthogonal ensemble (GOE), while a Poisson distribution is expected for localized states. It is convenient [27] to consider the ratio of consecutive level spacings $r^{(n)} = \min(\delta^{(n)},\delta^{(n+1)})/\max(\delta^{(n)},\delta^{(n+1)})$ with $\delta^{(n)} = E_n - E_{n-1}$ at a given eigenenergy E_n to discriminate between the two phases, as its disorder average changes from $r_{\text{GOE}} = 0.5307(1)$ [45] to $r_{\text{Poisson}} = 2 \ln 2 - 1 \simeq 0.3863$. This has been used in several works [21,27,28,31,36,39], averaging over a large part of the spectrum. Here, we compute r in an energy-resolved way in order to locate the MBL edge (Fig. 2).

Quite interestingly, the GOE-Poisson transition can also be captured by correlations between nearby eigenstates. We expect eigenfunctions to be "similar" ("different") in the ergodic (localized) regime. We quantify the degree of correlation by the Kullback-Leibler divergence (KLd) [46], defined by $\text{KL} = \sum_{i=1}^{\dim \mathcal{H}} p_i \ln(p_i/q_i)$, where $p_i = |\langle i|n \rangle|^2$ and $q_i = |\langle i|n' \rangle|^2$ are the moduli squared of the wave function coefficients of two nearby eigenstates $|n\rangle,|n'\rangle$ expressed in the computational basis $\{|i\rangle\}$ (here $\{S^z\}$). The KLd displays different behavior in the two phases (Fig. 2): We find $\text{KL}_{\text{GOE}} = 2$ [47], and $\text{KL}_{\text{Poisson}} \sim \ln(\dim \mathcal{H})$.

(b) Entanglement entropy (EE). Beyond level statistics, EE provides a quantitative tool to characterize how information is spread from one part of the system to another [8]. In the ergodic regime satisfying the ETH, the reduced density matrix ρ_A of a typical eigenstate is expected to be thermal, yielding a volume-
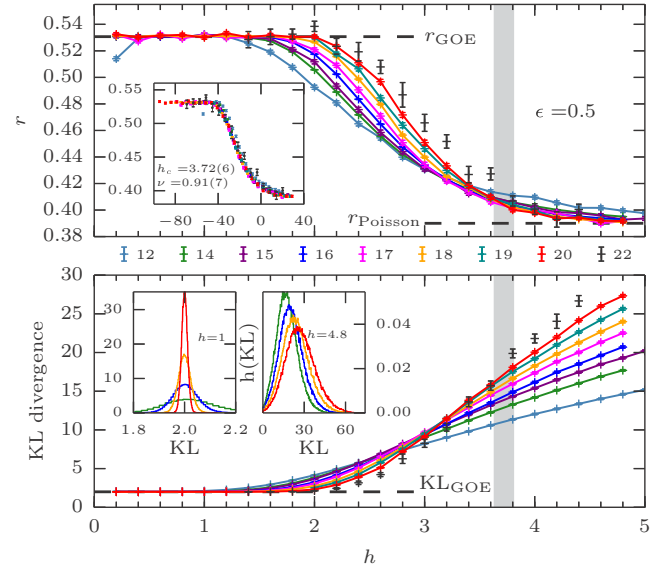

FIG. 2. (Color online) Adjacent gap ratio (top) and Kullback Leibler divergence (bottom) as a function of disorder strength in the spectrum center $\epsilon = 0.5$. Insets: (top) data collapse used to extract the critical disorder strength h_c and exponent ν. The h axis is transformed by $(h - h_c)L^{1/\nu}$; (bottom) distribution of KLd in both phases.

law scaling (with the subsystem A size) for the entanglement entropy $S^E = -\text{Tr}\rho_A \ln \rho_A$. Conversely, localized eigenstates display a much smaller entanglement, expected to cross over towards an area-law scaling [8,21] when the subsystem size exceeds the localization length. These different scalings of S^E allow one to distinguish both regimes (Fig. 3). In the same spirit, we expect bipartite fluctuations of the subsystem magnetization S_A^z [48] $\mathcal{F} = \langle (S_A^z)^2 \rangle - \langle S_A^z \rangle^2$ to exhibit similar scaling (Fig. 4).

(c) Hilbert-space localization. Another characterization of MBL relies on inverse participation ratios and associated participation entropies (PE), traditionally used in the context of single particle localization [49–51] and recently for many-body physics [52,53]. Here the localization is studied in the Hilbert space (of dimension $\dim \mathcal{H}$) of spin configurations via the disorder average PEs S_q^P, defined for any eigenstate $|n\rangle$ represented in the $\{S^z\}$ basis by $S_q^P(|n\rangle) = \frac{1}{1-q} \ln \sum_i p_i^q$ $[S_1^P(|n\rangle) = -\sum_i p_i \ln p_i]$. We generically find eigenstates to be delocalized *in both* regimes with qualitatively different features. In the ergodic regime, we obtain a leading scaling $S_q^P = a_q \ln(\dim \mathcal{H})$ with $a_q \approx 1 \forall q$ (see color coding of a_1 in Fig. 1). In the localized phase, PE also grows with system size (Fig. 5), but much slower with $a_q \ll 1$, or $a_q = 0$ within error bars and a slow log divergence $S_q^P = l_q \ln(\ln \dim \mathcal{H})$, indicating a nontrivial multifractal behavior.

Numerical method. The complete diagonalization of the not translation invariant Hamiltonian equation (1) is out of reach for system sizes $L \gtrsim 18$ spins. Therefore, we use an approach successful for the Anderson localization problem (see, e.g., Ref. [51]) and restrict ourselves to certain energy slices in the spectrum by using a shift-invert spectral transformation $(\mathbf{H} - E\mathbf{1})^{-1}$. In the transformed problem, it is easy to apply
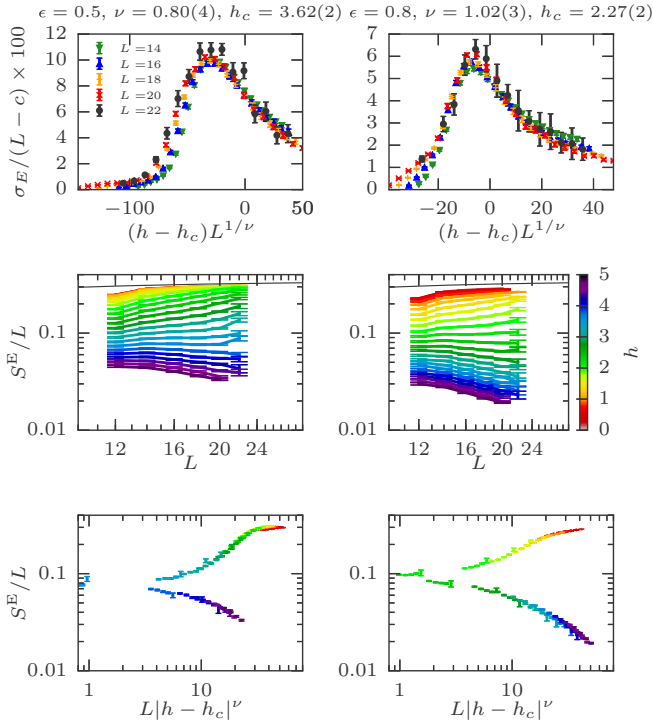
FIG. 3. (Color online) Entanglement entropy per site S^{E}/L and its variance σ_E, as a function of system size L for different disorder strengths in the middle of the spectrum (left) and in the upper part (right). The volume-law scaling leading to a constant S^{E}/L for weak disorder contrasts with the area law (signaled by a decreasing S^{E}/L) at larger disorder. Black line: S^{E}/L for a random state [58]. Close to the transition, the prefactor of the volume law is expected to converge only for larger system sizes.

Krylov space methods [54] to compute the eigenpairs closest to the shift energy E.

For each disorder realization, we first calculate the extremal eigenenergies E_0 and $E_{\max}$ used to define the normalized energy target $\epsilon = (E - E_{\max})/(E_0 - E_{\max})$ (we considered the $S^z = 0$ sector of even-sized $L = 12,14,16,18,20,22$ and $S^z = 1$ sector of $L = 15,17,19$). The shift-invert method,
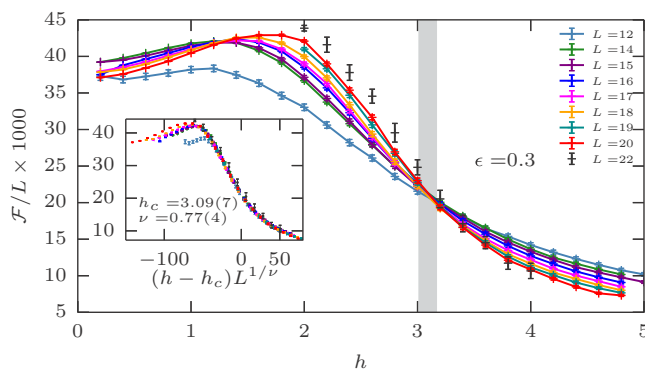

FIG. 4. (Color online) Bipartite fluctuations of half-chain magnetization as a function of disorder strength at $\epsilon = 0.3$. Inset: Data collapse using the best estimates for the critical disorder strength $h_c = 3.09(7)$ and $\nu = 0.77(4)$.
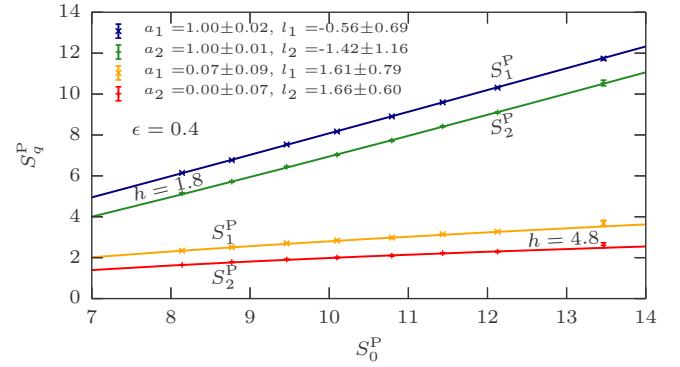

FIG. 5. (Color online) Participation entropy as a function of $S_0^{\mathrm{P}} = \ln(\dim \mathcal{H})$ for $q = 1,2$ and $\epsilon = 0.4$. In the ergodic phase ($h = 1.8$), S_q^{P} grows linearly with S_0^{P} while the linear scaling term vanishes within our error bars in the localized regime ($h = 4.8$). Our fits (solid lines; see text) constrain $a_q \in [0,1]$ and yield a logarithmic scaling prefactor $\bar{l}_q \approx 2(1)$ at $h = 4.8$, consistent with a (slow) growth of S_q^{P} with system size in the localized phase.

based on a massively parallel LU decomposition [55,56], is then used to calculate at least 50 eigenpairs with energy densities closest to the targets $\epsilon = \{0.05, 0.1, \ldots, 0.95\}$. Note that this is a much more demanding computational task than for the Anderson problem, as the number of off-diagonal elements of H scales with L. We use at least 1000 disorder realizations for each L (except for $L = 22$ where we accumulated between 50 and 250 samples). For each ϵ, observables are calculated from the corresponding eigenvectors and averaged over target packets and disorder realizations for each value of the disorder strength h. As eigenvectors of the same disorder realization are correlated, we found it crucial [51] to bin quantities over all eigenstates of the same realization, and then compute the standard error over these bin averages, in order not to underestimate error bars. Investigating numerous quantities allows one to check the consistency of our analysis and conclusions.

Results and finite-size scaling analysis. We discuss the transition between GOE and Poisson statistics, first using the consecutive gap ratio $\bar{r}$, shown in Fig. 2 (top) for $\epsilon = 0.5$. When varying the disorder strength h, we clearly see a crossing around $h_c \sim 3.7$ between the two limiting values. This crossing can be analyzed using a scaling form $g[L^{1/\nu}(h - h_c)]$ which allows a collapse of the data onto a single universal curve (see inset), yielding $h_c = 3.72(6)$ and $\nu = 0.91(7)$ (see details of fitting procedure and error bar estimates in Supplemental Material [57]).

The above defined KLd, computed for two eigenstates randomly chosen at the same energy target ϵ and averaged over disordered samples, also displays a crossing between the two limit scalings $\mathrm{KL}_{\mathrm{GOE}} = 2$ and $\mathrm{KL}_{\mathrm{Poisson}} \sim \ln(\dim \mathcal{H})$ (Fig. 2, bottom). A data collapse is very difficult to achieve for KL due to a large drift of the crossing points. Nevertheless, the distributions of KL plotted in insets, display markedly different features. The perfect Gaussian distribution in the ergodic phase (at $h = 1$) around the GOE mean value of 2 with a variance decreasing with L provides strong evidence that the statistical behavior of the *eigenstates* is well described by

GOE, extending its applicability beyond simple level statistics. In the MBL regime ($h = 4.8$), the behavior is completely different as variance and mean both increase with L.

We now turn to the entanglement entropy for a real space bipartition at $L/2$ (L even). Shown for two targets $\epsilon = 0.5$ and 0.8, the transition is signaled (Fig. 3) by a change in the EE scalings from volume law $S^{\mathrm{E}}/L \rightarrow$ constant for $h < h_c$ to area law with $S^{\mathrm{E}}/L \rightarrow 0$ for $h > h_c$. Assuming a volume-law scaling at the critical point [59], we perform a collapse of S^{E}/L to the form $g[L^{1/\nu}(h - h_c)]$ (Fig. 3, bottom panel) giving estimates for the critical disorder h_c and exponent ν consistent with other results (see Supplemental Material [57]). Furthermore, as recently argued [32], the standard deviation of the entanglement entropy displays a maximum at the MBL transition. A scaling collapse of the form $\sigma_E = (L - c)g[L^{1/\nu}(h - h_c)]$ (with c an unknown parameter and the previous estimates of ν and h_c from collapse of S^{E}/L) works particularly well (top panel of Fig. 3).

Perhaps more accessible to experiments, bipartite fluctuations $\mathcal{F}$ of subsystem magnetization (taken here to be a half-chain $L/2$) have a similar behavior. Being simply the Curie constant of the subsystem, we also expect thermal extensivity (subextensive response) in the ergodic (localized) regime. This is clearly checked in Fig. 4 for $\epsilon = 0.3$ where $\mathcal{F}/L$ has a crossing point at the disorder-induced MBL transition. A data collapse (inset of Fig. 4) is also possible for $\mathcal{F}/L = g[L^{1/\nu}(h - h_c)]$, giving $h_c = 3.09(7)$ and $\nu = 0.77(4)$, consistent with estimates from other quantities (Fig. 1). Finally, we also performed an analysis of the dynamic fraction f of an initial spin polarization [28], and obtained similar consistent scaling (see Supplemental Material [57] and Fig. 1).

The disordered many-body system can be mapped onto a single particle problem on the complex graph spanned by the Hilbert space whose $\dim \mathcal{H}$ vertices are the basis states, which are connected by spin-flip terms in Eq. (1). The average coordination of each node is $z \sim L$ and the random potential has a Gaussian distribution of variance $\sigma_h \sim h\sqrt{L}$, meaning that the effective connectivity grows faster than the disorder strength. Using recent results on Anderson localization on Bethe lattices at large connectivity [60], we do not expect genuine Hilbert-space localization at any finite disorder. This argument is corroborated by our numerical results for the PE S_q^{P} (Fig. 5) which are always found to increase with $S_0^{\mathrm{P}} \equiv \ln(\dim \mathcal{H})$, albeit much more slowly in the localized regime. Analysis of various fits of the form

$S_q^{\mathrm{P}} = a_q S_0^{\mathrm{P}} + l_q \ln(S_0^{\mathrm{P}}) + o(S_0^{\mathrm{P}})$ indicate that $a_q \simeq 1 \, \forall q$ in the ergodic regime (with possibly small negative l_q corrections) as seen in the color scale of Fig. 1, in contrast to Anderson localization on the Bethe lattice [61]. In the localized regime, we obtain essentially similar fit qualities with $a_q \ll 1$ (see typical numbers in Fig. 5), or $a_q = 0$ and $l_q > 0$ (the slow growth of S_q^{P} and our limited system sizes do not allow one to separate these two possibilities).

Discussions and conclusions. Using various estimates for the MBL transition, our large-scale energy-resolved ED results indicate the existence of an extensive many-body mobility edge in the excitation spectrum (Fig. 1) of the random field Heisenberg chain. Furthermore, we show that the ergodic regime has full features of a metallic phase (with $a_q = 1$ and GOE statistics for both energy levels *and* the wave-function coefficients), and that the localized many-body states do not exhibit a true Hilbert-space localization for configuration spaces up to dim $\mathcal{H} \sim 7 \times 10^5$ [62]. Our detailed finite-size scaling analysis (Supplemental Material [57]) provides a consistent estimate of a characteristic length diverging as $|h - h_c|^{-\nu}$ with $\nu = 0.8(3)$ through the full phase diagram. This estimate of the exponent ν appears to violate the Harris-Chayes [63,64] criterion $\nu \geqslant 2/d$ (see also Ref. [32]) within the system sizes used. This is quite intriguing given that for the same size range, the location of the critical point is consistent for all various estimates used (see Fig. 1). This opens new questions on the finite-size scaling and/or corrections to scaling at the MBL transition which may not follow [27,28] standard forms.

Besides these results for the particular model, Eq. (1), we believe that the numerical techniques (massively parallel energy-resolved diagonalization) and new indicators of the ergodic-localized transition (eigenstate correlations or bipartite fluctuations) introduced here will be useful in a large number of contexts related to MBL or ETH. In particular, the obtention of exact eigenvectors on fairly large systems will be crucial to quantify the effectiveness of encoding localized states as matrix product states, as recently advocated [65–67].

[1] L. Fleishman and P. W. Anderson, Phys. Rev. B **21**, 2366 (1980).

[2] B. L. Altshuler, Y. Gefen, A. Kamenev, and L. S. Levitov, Phys. Rev. Lett. **78**, 2803 (1997).

[3] P. Jacquod and D. L. Shepelyansky, Phys. Rev. Lett. **79**, 1837 (1997).

[4] B. Georgeot and D. L. Shepelyansky, Phys. Rev. Lett. **81**, 5129 (1998).

[5] I. V. Gornyi, A. D. Mirlin, and D. G. Polyakov, Phys. Rev. Lett. **95**, 206603 (2005).

[6] D. M. Basko, I. L. Aleiner, and B. L. Altshuler, Ann. Phys. (N.Y.) **321**, 1126 (2006).

[7] P. W. Anderson, Phys. Rev. **109**, 1492 (1958).

[8] R. Nandkishore and D. A. Huse, arXiv:1404.0686.

[9] E. Altman and R. Vosk, arXiv:1408.2834.

[10] J. M. Deutsch, Phys. Rev. A **43**, 2046 (1991).

[11] M. Srednicki, Phys. Rev. E **50**, 888 (1994).

[12] M. Rigol, V. Dunjko, and M. Olshanii, Nature (London) **452**, 854 (2008).

[13] R. Nandkishore, S. Gopalakrishnan, and D. A. Huse, Phys. Rev. B **90**, 064203 (2014).

[14] M. Serbyn, M. Knap, S. Gopalakrishnan, Z. Papić, N. Y. Yao, C. R. Laumann, D. A. Abanin, M. D. Lukin, and E. A. Demler, Phys. Rev. Lett. **113**, 147204 (2014).

[15] M. P. Kwasigroch and N. R. Cooper, Phys. Rev. A **90**, 021605 (2014).

[16] N. Y. Yao, C. R. Laumann, S. Gopalakrishnan, M. Knap, M. Mueller, E. A. Demler, and M. D. Lukin, Phys. Rev. Lett. **113**, 243002 (2014).

[17] R. Vasseur, S. A. Parameswaran, and J. E. Moore, arXiv:1407.4476.

[18] D. A. Huse, R. Nandkishore, V. Oganesyan, A. Pal, and S. L. Sondhi, Phys. Rev. B **88**, 014206 (2013).

[19] Y. Bahri, R. Vosk, E. Altman, and A. Vishwanath, arXiv:1307.4092.

[20] A. Chandran, V. Khemani, C. R. Laumann, and S. L. Sondhi, Phys. Rev. B **89**, 144201 (2014).

[21] B. Bauer and C. Nayak, J. Stat. Mech.: Theory Exp. (2013) P09005.

[22] R. Vosk and E. Altman, Phys. Rev. Lett. **112**, 217204 (2014).

[23] D. A. Huse, R. Nandkishore, and V. Oganesyan, Phys. Rev. B **90**, 174202 (2014).

[24] M. Serbyn, Z. Papić, and D. A. Abanin, Phys. Rev. Lett. **111**, 127201 (2013).

[25] V. Ros, M. Müller, and A. Scardicchio, Nucl. Phys. B **891**, 420 (2015).

[26] A. Chandran, I. H. Kim, G. Vidal, and D. A. Abanin, arXiv:1407.8480.

[27] V. Oganesyan and D. A. Huse, Phys. Rev. B **75**, 155111 (2007).

[28] A. Pal and D. A. Huse, Phys. Rev. B **82**, 174411 (2010).

[29] M. Žnidarič, T. Prosen, and P. Prelovšek, Phys. Rev. B **77**, 064426 (2008).

[30] E. Canovi, D. Rossini, R. Fazio, G. E. Santoro, and A. Silva, Phys. Rev. B **83**, 094431 (2011).

[31] E. Cuevas, M. Feigel'Man, L. Ioffe, and M. Mezard, Nat. Commun. **3**, 1128 (2012).

[32] J. A. Kjäll, J. H. Bardarson, and F. Pollmann, Phys. Rev. Lett. **113**, 107204 (2014).

[33] A. De Luca and A. Scardicchio, Europhys. Lett. **101**, 37003 (2013).

[34] S. Iyer, V. Oganesyan, G. Refael, and D. A. Huse, Phys. Rev. B **87**, 134202 (2013).

[35] D. Pekker, G. Refael, E. Altman, E. Demler, and V. Oganesyan, Phys. Rev. X **4**, 011052 (2014).

[36] S. Johri, R. Nandkishore, and R. N. Bhatt, arXiv:1405.5515.

[37] J. H. Bardarson, F. Pollmann, and J. E. Moore, Phys. Rev. Lett. **109**, 017202 (2012).

[38] F. Andraschko, T. Enss, and J. Sirker, Phys. Rev. Lett. **113**, 217201 (2014).

[39] C. R. Laumann, A. Pal, and A. Scardicchio, Phys. Rev. Lett. **113**, 200405 (2014).

[40] J. M. Hickey, S. Genway, and J. P. Garrahan, arXiv:1405.5780.

[41] A. Nanduri, H. Kim, and D. A. Huse, Phys. Rev. B **90**, 064201 (2014).

[42] Y. Bar Lev and D. R. Reichman, Phys. Rev. B **89**, 220201 (2014).

[43] We note that dynamics after a quench can be investigated on fairly large systems using methods that benefit from the low rise of entanglement in a MBL system [29,37,38].

[44] M. L. Mehta, *Random Matrices* (Academic, Boston, 1991).

[45] Y. Y. Atas, E. Bogomolny, O. Giraud, and G. Roux, Phys. Rev. Lett. **110**, 084101 (2013).

[46] S. Kullback and R. A. Leibler, Ann. Math. Statist. **22**, 79 (1951).

[47] We found this numerically for eigenvectors of random matrices in the GOE ensemble, inspiring an analytical proof [O. Giraud (private communication)].

[48] H. F. Song, S. Rachel, C. Flindt, I. Klich, N. Laflorencie, and K. Le Hur, Phys. Rev. B **85**, 035409 (2012).

[49] R. J. Bell, Rep. Prog. Phys. **35**, 1315 (1972).

[50] F. Wegner, Z. Phys. B **36**, 209 (1980).

[51] A. Rodriguez, L. J. Vasquez, K. Slevin, and R. A. Römer, Phys. Rev. B **84**, 134209 (2011).

[52] D. J. Luitz, F. Alet, and N. Laflorencie, Phys. Rev. Lett. **112**, 057203 (2014).

[53] D. J. Luitz, N. Laflorencie, and F. Alet, J. Stat. Mech.: Theory Exp. (2014) P08007.

[54] V. Hernandez, J. E. Roman, and V. Vidal, ACM Trans. Math. Software **31**, 351 (2005).

[55] P. R. Amestoy, I. S. Duff, J. Koster, and J.-Y. L'Excellent, SIAM J. Matrix Anal. Appl. **23**, 15 (2001).

[56] P. R. Amestoy, A. Guermouche, J.-Y. L'Excellent, and S. Pralet, Parallel Comput. **32**, 136 (2006).

[57] See Supplemental Material at http://link.aps.org/supplemental/10.1103/PhysRevB.91.081103 for details on fitting procedures and additional data for the dynamical spin fraction.

[58] D. N. Page, Phys. Rev. Lett. **71**, 1291 (1993).

[59] T. Grover, arXiv:1405.1471.

[60] G. Biroli, G. Semerjian, and M. Tarzia, Progr. Theor. Phys. Suppl. **184**, 187 (2010).

[61] A. De Luca, B. L. Altshuler, V. E. Kravtsov, and A. Scardicchio, Phys. Rev. Lett. **113**, 046806 (2014).

[62] We cannot exclude a different multifractal behavior $0 < a_q < 1$ very close to the transition.

[63] A. B. Harris, J. Phys. C: Solid State Phys. **7**, 1671 (1974).

[64] J. T. Chayes, L. Chayes, D. S. Fisher, and T. Spencer, Phys. Rev. Lett. **57**, 2999 (1986).

[65] M. Friesdorf, A. H. Werner, W. Brown, V. B. Scholz, and J. Eisert, arXiv:1409.1252.

[66] A. Chandran, J. Carrasquilla, I. H. Kim, D. A. Abanin, and G. Vidal, arXiv:1410.0687.

[67] D. Pekker and B. K. Clark, arXiv:1410.2224.